SINUOSITY AS A MEASURE OF MIDDLE TROPOSPHERIC WAVINESS

by

Jonathan E. Martin[1], Stephen J. Vavrus[2], Fuyao Wang[2], and Jennifer A. Francis[3]

[1]Department of Atmospheric and Oceanic Sciences, University of Wisconsin-Madison
[2]Center for Climatic Research, University of Wisconsin-Madison
[3]Department of Marine and Coastal Sciences, Rutgers University

Submitted to *Journal of Climate*: February 16, 2016

ABSTRACT

Despite the importance of synoptic- to planetary-scale atmospheric waves in the production of organized mid-latitude weather systems, no single metric for quantifying the waviness of the large-scale circulation is widely employed. The concept of sinuosity, borrowed from geomorphology, is introduced as a means of measuring the waviness of the mid-tropospheric flow using 500 hPa geopotential height contours. A simple method for calculating the sinuosity of the flow is presented and several broad characteristics of the flow are discussed.

First, the circulation is characterized by a maximum in waviness in the summer and a minimum in winter. Second, weakening (strengthening) of the mid-tropospheric zonal flow is shown to be associated with increased (decreased) waviness. Third, a strong negative correlation is found between the observed daily sinuosity and the daily Arctic Oscillation (AO) index in the cold season. Additionally, the DJF average sinuosity is shown to be highly correlated with the seasonal average AO index, suggesting that physical mechanisms that reduce (increase) the poleward height gradient, and correspondingly weaken (strengthen) the mid-latitude westerlies, may also encourage increased (reduced) waviness. The use of this metric to examine changes in the complexion of mid-latitude waviness in a changing climate is discussed.

1. Introduction

In recognition of the prominent role played by the mid-latitude westerlies in the general circulation of the Earth's atmosphere, Rossby and collaborators (1939) introduced the concept of the "zonal index"[1] as a measure of the strength of the zonal westerlies. Subsequent work by Namias (1950) examined what appeared to be a characteristic decline and recovery of the westerlies each winter in what he termed the "index cycle". This work represented the culmination of a series of investigations (e.g. Namias 1947a,b, Willett 1948, Wexler 1948) linking changes in the hemispheric circulation (evident in changes in the zonal index) to the equatorward movement of cold air during boreal winter. Central to this idea was the notion that strong, zonally oriented mid- to upper-tropospheric westerlies act to contain cold air at high latitudes so that cold-air outbreaks are afforded when the zonality of the flow relaxes.

The development of blocking ridges substantially interrupts the zonality of the flow and so has become a topic of considerable inquiry (e.g. Elliot and Smith 1949, Rex 1950ab, White and Clark 1975, Egger 1978, Austin 1980, Legenäs and Øakland 1983, Dole and Gordon 1983, Lupo and Smith 1995, Shabbar et al. 2001, Pelly and Hoskins 2003, Schwierz et al. 2004, Woollings et al. 2011, Masato et al. 2013, Barnes et al. 2014, Davini et al. 2014). Another feature at the center of studies of hemispheric circulation variability has been the circumpolar vortex (CPV) (e.g. Markham 1985, Angell 1998, Davis and Benkovic 1992, Burnett 1993, Frauenfeld

[1] Originally defined at sea-level as the average geostrophic wind in the latitude belt 35°N to 55°N. It is commonly evaluated aloft as well.

and Davis 2003, Rohli et al. 2005, Wrona and Rohli 2007). As noted by Frauenfeld and Davis (2003), assessment of variability in the size, strength and waviness of the circulation can all be considered in terms of measurable characteristics of the CPV.

To our knowledge, only two studies of the variability of the CPV have directly assessed the waviness of the mid-tropospheric flow. Rohli et al. (2005) borrowed a measure from fluvial geomorphology – the circularity ratio (R_c) – to quantify the waviness of the 5460m isohypse at 500 hPa (recommended by the study of Frauenfeld and Davis 2003) for the month of January from 1959-2001. Wrona and Rohli (2007) extended this analysis to DJF for each of those 43 cold seasons and added analyses of the months of April, July, and October in order to uncover aspects of the seasonality of the CPV, as depicted by this single 500 hPa isohypse.

High impact mid-latitude weather events and regimes are often associated with large-amplitude planetary waves, as such patterns are dynamically linked to robust cyclogenesis and anticyclogenesis events as well as the development of blocked flows. In spite of this well-known relationship, no particular metric for quantifying the waviness of the circulation is widely used. Recent studies employing gridded reanalysis data sets have offered reasonable suggestions. Francis and Vavrus (2012) and Barnes (2013) incorporated measures of the maximum meridional extent of 500 hPa isohypses (on both seasonal and daily time scales) as a means of examining interannual trends in the complexion of middle tropospheric waves. Screen and Simmonds (2013) employed a Fourier decomposition to first characterize both the meridional and zonal amplitudes of waves in the mid-latitude

middle troposphere, and then examine temporal changes in these characteristics. Among the various specific metrics applied elsewhere are effective diffusivity, finite-amplitude wave activity (FAWA) and its recent regional generalization, local finite-amplitude wave activity (LWA).

Perhaps the best physical analog for sinuosity is effective diffusivity, introduced by Nakamura (1996) and Winters and D'Asaro (1996) in the context of chemical transport studies. Effective diffusivity can be regarded as a measure of the complexity of the geometric structure of the tracer (Haynes and Shuckburgh, 2000a,b). By converting the area enclosed by a specified tracer concentration to an equivalent latitude (ϕ_e), Nakamura (1996) showed that mixing in non-divergent flows is governed by diffusion only when the effective diffusion, K_{eff}, is given by

$$K_{eff} = \frac{\kappa L_{eq}^{\ 2}(\phi_e, t)}{(2\pi R\cos\phi_e)^2}$$

where $L_{eq}(\phi_e,t)$ is the equivalent length of a tracer contour and $2\pi R\cos\phi_e$ is the length of its associated equivalent latitude circle on the sphere. Thus, the "wavier" the tracer contours, the larger K_{eff}.

Finite-amplitude wave activity (FAWA) is defined in terms of the integrated areal displacement of a quasi-geostrophic potential vorticity (PV) contour from its equivalent latitude and has been used primarily to diagnose the dynamics of eddy-mean flow interaction (e.g., Nakamura and Solomon 2010, Nakamura and Zhu 2010). More recently, FAWA has been generalized into LWA, a regional metric that identifies and characterizes the synoptic- and large-scale environments associated

110 with high-amplitude wave events such as atmospheric blocking and cold air
111 outbreaks (Huang and Nakamura 2015, Chen et al. 2015).

112 In the present paper we appropriate a measure common in geomorphology –
113 *sinuosity* – to measure the waviness of the mid-tropospheric flow using 500 hPa
114 geopotential height contours. As will be shown, calculation of this simple quantity
115 ensures that any departure from zonality in geostrophic streamlines, *not only the*
116 *most extreme departures*, is incorporated into a metric of hemispheric waviness. A
117 seasonality in the sinuosity of the flow is demonstrated, with a maximum in summer
118 and minimum in winter. Through consideration of a 500 hPa zonal index[2], a
119 characteristic weakening of the mid-tropospheric zonal wind in association with an
120 increase in sinuosity is demonstrated. Additionally, a strong negative correlation is
121 found between the observed daily sinuosity and the daily Arctic Oscillation (AO)
122 index in the cold season. Further, the winter (DJF) average sinuosity is shown to be
123 highly correlated with the seasonal average AO, suggesting that physical
124 mechanisms that reduce (increase) the poleward height gradient and
125 correspondingly weaken (strengthen) the mid-latitude westerlies, may also foster
126 increased (reduced) waviness.

127 The purpose of this paper is to introduce a new tool for assessing changes in
128 the complexion of the large-scale circulation and to demonstrate fundamental
129 aspects of its utility. Accordingly, the paper is organized in the following manner.
130 In Section 2 we define sinuosity and describe both the method and data set used to

[2] The daily 500 hPa zonal index is calculated as the zonal average of the westerly geostrophic wind at 500 hPa in the latitude belt 35°-55°N.

131 calculate it. Aspects of the annual cycle in sinuosity, along with an emphasis on
132 analysis of a time series of the previous 66 winter seasons, are presented in Section
133 3. The relationship between cold-season time series of sinuosity and the AO are also
134 considered in that section. Finally, a summary and discussion of the results,
135 including suggestions for future research, are offered in Section 4.

136 **2. Data and Methodology**

137 Morphological aspects of the meanders of rivers and streams is a subject in
138 fluvial geomorphology. A simple measure of such meanders is known as sinuosity
139 which is the ratio of the length of a segment of a stream to the length of the shortest
140 distance between the endpoints of the segment (Leopold et al. 1964). A schematic
141 example is given in Fig. 1. The extension of this idea employed in the present study
142 depends upon calculation of the length of, and the area enclosed by, a given 500 hPa
143 geopotential height contour (isohypse). Cutoff portions of any isohypse (i.e. cutoff
144 lows or highs) are easily included in our measure of sinuosity because such features
145 occupy a measurable area and their perimeters have finite lengths. We consider the
146 waviness in a given mid-latitude flow to be a measure of the departure of its
147 streamlines from zonality. Therefore, determination of the sinuosity of the flow
148 along a geostrophic streamline (i.e., isohypse) begins by calculating the area
149 enclosed by the given isohypse. Next, we compute an equivalent latitude for that
150 isohypse. The equivalent latitude is that latitude poleward of which the area is

151 equal to the area enclosed by the given isohypse[3]. Finally, the sinuosity is defined as
152 the ratio of the length of the given 500 hPa isohypse to the circumference of its
153 equivalent latitude circle. An example is shown in Fig. 2. It follows from the
154 definition that the minimum value of sinuosity is 1.0 which describes a purely zonal
155 streamline (i.e., no waviness).

156 It has been suggested that shifting isohypses poleward in a warmer climate
157 might give rise to the illusion, when using sinuosity as a metric, of a change in
158 waviness when none is actually occurring. In order to evaluate this concern we
159 conducted a series of simple numerical experiments in which the sinuosity of
160 hypothetical isohypses, characterized by a varying number of deep and shallow
161 square waves, were carefully examined. The simplest case of a single modest square
162 wave is shown in Fig. 3. Keeping the aspect ratio of the square wave constant upon
163 moving the isohypse from 35° to 40°N results in an 8.9° latitudinal depth at 40°N
164 compared to the original 10° at 30°N. The poleward encroachment of this
165 waveform results in a 0.24% increase in sinuosity at the higher latitude. We suggest
166 this is well small enough to ensure that the utility of sinuosity as a metric of
167 waviness is not compromised. We also note that recent work by Bezeau et al.
168 (2014) demonstrates that the daily climatological variability in Northern
169 Hemisphere 500 hPa height anomalies is significantly greater than the long term

[3] If A is the area enclosed by a given isohypse, then the equivalent latitude, ϕ_e, is given by $\phi_e = \arcsin[1 - \frac{A}{2\pi R_e^2}]$, where R_e is the radius of the Earth. Reference to an equivalent latitude is reminiscent of an aspect of the measure of eddy amplitude employed by Nakamura and Zhu (2010) and Nakamura and Solomon (2010, 2011) in their development of a diagnostic formulation for finite-amplitude wave activity.

increase in heights resulting from Arctic amplification. Additional support for allaying the aforementioned concern derives from the fact that sinuosity can also be described as a function of latitude (see Appendix).

Though many prior investigations of the variability of the mid-tropospheric circulation have considered the area of the circumpolar vortex, only Rohli et al. (2005) and Wrona and Rohli (2007) explicitly considered the waviness. They did so using a measure called the circularity ratio (R_c) defined as the area enclosed within a given isohypse divided by the area poleward of a zonal ring whose perimeter is identically the length of the given isohypse. They applied this measure to a single 500 hPa isohypse (546 dm) for 43 cold seasons (DJF) using observed mean monthly 500 hPa geopotential height analyses on a 5° x 5° latitude/longitude grid from NCAR's Monthly Northern Hemisphere Tropospheric Analysis.[4] Their choice of the 5460 m isohypse was motivated by the desire to consistently sample the size and shape of the circumpolar vortex within the main belt of the westerlies. As described below, our study builds on these pioneering efforts to quantify atmospheric waviness by expanding the analysis in time and space and by applying a more physically based morphometric parameter.

We employ the NCEP/NCAR reanalysis (NRA) data (Kalnay et al. 1996). Note that while direct comparisons of reanalysis values to observations is problematic owing to lack of independent measures, the upper-level circulation in the NRA has been found to be very similar to that of the reanalysis by the European Centre for

[4] These data are available at http://dss/ucar/edu/datasets/ds085.1

191 Medium Range Weather Forecasts (Archer and Caldeira, 2008) and other reanalyses
192 by Davini (2013). These data are available 4 times daily on a global 2.5° x 2.5° grid
193 and are derived from a frozen state-of-the-art global assimilation system in
194 conjunction with a database that includes in-situ and remotely sensed data (when
195 available) both at the surface and at levels through the troposphere and
196 stratosphere. The present study calculates the sinuosity of a collection of individual
197 500 hPa isohypses in a domain covering 20°N to 90°N, using daily average 500 hPa
198 heights constructed from the four times daily data, from 1 January 1948 to 28
199 February 2014. In addition to calculating the sinuosity of individual 500 hPa
200 isohypses, we also calculate the aggregate sinuosity of a set of 5 isohypses (576, 564,
201 552, 540, and 528 dm) in which the maximum 500 hPa geostrophic wind resides
202 throughout the year. The aggregate sinuosity at a given time is simply the ratio of
203 the sum of the lengths of all 5 isohypses to the sum of the circumferences of the 5
204 equivalent latitude circles at that time[5].

205 A note regarding the differences between circularity ratio and sinuosity as
206 separate measures of the waviness is warranted. Calculation of circularity ratio for
207 a given isohypse requires determination of a latitude, ϕ_P, at which the length of a
208 zonal streamline is equal to the length of the isohypse. Since the *areal extent*, not

[5] One can choose any set of consecutive isohypses to produce an aggregate sinuosity. The choice made here is motivated by a desire to sample in the main belt of the westerlies. The aggregate sinuosity here is given by $S_5 = \frac{[L_{576} + L_{564} + L_{552} + L_{540} + L_{528}]}{[EL_{576} + EL_{564} + EL_{552} + EL_{540} + EL_{528}]}$ where L is the length of the indicated isohypse and EL is the length of its corresponding equivalent latitude circle. As opposed to a simple arithmetic mean of the individual sinuosity of the 5 isohypses, S_5 describes the integrated waviness of the geostrophic flow in the region spanning the selected isohypses.

the length, of a given isohypse is directly related to a first order atmospheric variable (i.e. average temperature in the underlying troposphere via the hypsometric relationship), we submit that sinuosity is a more physically relevant measure of the waviness. Furthermore, the present analysis, in contrast to those by Rohli et al. (2005) and Wrona and Rohli (2007), considers a complete annual cycle in waviness, relates the waviness metric to an important mode of large-scale atmospheric variability (the Arctic Oscillation), and incorporates a range of isohypses to more comprehensively characterize the complexion of middle tropospheric waves across a broader extratropical domain. The mathematical relationship between the two measures is presented in the Appendix.

3. Results

In order to examine the waviness of the 500 hPa flow in as comprehensive a manner as possible, the following analysis is split into two broad categories. We first consider the results of the 5 contour aggregate sinuosity calculations and then move to evaluation of the characteristics of individual isohypses.

a. Aggregate sinuosity

The 500 hPa aggregate sinuosity analysis presented here considers the 576, 564, 552, 540, and 528 dm geopotential height contours and will be referred to as S_5[6]. Each of these contours encloses a certain amount of area. Equal area is contained poleward of an equivalent latitude (ϕ_{EQ}) and the length of the zonal ring at

[6] The correlation of the seasonal (DJF) average zonal index with seasonal average S_5 is -0.651.

ϕ_{EQ} represents the shortest possible perimeter that can enclose the given amount of area. The contour length of a given isohypse is determined by summing its segments in each 2.5° x 2.5° grid box calculated using the Spherical Law of Cosines formula;

$$L = \arccos[\sin\phi_1 \sin\phi_2 + \cos\phi_1 \cos\phi_2 \cos(\lambda_2 - \lambda_1)]R_e$$

where (ϕ_1, λ_1) and (ϕ_2, λ_2) represent the latitude and longitude coordinates where the given isohypse intersects the boundaries of a grid box and R_e is the radius of the Earth.

The analysis presented here focuses on the winter (DJF) as it is during this season that the Northern Hemisphere mid-latitude flow is at its energetic peak. The 66-year time series of DJF-average aggregate sinuosity is shown in Fig. 4. Over the course of this time series no systematic trend is evident though since ~1990 a slight, and statistically insignificant, upward trend in the aggregate sinuosity is apparent.

The exceptionally high values of sinuosity in 2009-10 and 2010-11, suggest a possible relationship with the Arctic Oscillation (AO), which reached its strongest negative phase in winter 2009-10. Because mid-latitude circulation during the positive (negative) phase of the AO tends to be anomalously zonal (wavy), sinuosity should be able to capture this behavior quantitatively. Employing the daily Arctic Oscillation (AO) time series from 1 December 1950 to present, the correlation between the daily aggregate sinuosity of the 500 hPa flow and the AO index for each DJF season since 1950-51 is shown in Fig. 5a. Twenty-three of 64 years exhibit a strong inverse relationship ($r \leq -0.6$) between the AO index and our measure of

sinuosity. In 43 of the 64 years r ≤ -0.4, indicating a moderate relationship between the two time series. This relationship is further illustrated in Fig. 5b where daily AO is compared against daily aggregate sinuosity for every DJF day in the time series. The two measures are correlated at -0.43 at the 99.9% significance level. Additional insight into this relationship arises from consideration of the seasonal average AO index compared to the seasonal average sinuosity, as shown in Fig. 6. It is clear that enhanced waviness in the 500 hPa flow is associated with a negative AO as the two time series are correlated at r = -0.52 (significant above the 99% confidence level).

Another, less direct, inference regarding waviness of the middle-latitude flow can be discerned from the zonal index. Figure 7a shows the time series of the correlation between the daily aggregate sinuosity (S_5) and the zonal index (ZI) for each DJF season since 1948-49. In 26 (45) of the 66 years the two time series are correlated at r ≤ -0.6 (-0.4) though, as with the AO correlation just described, in nearly 1/3 of seasons the relationship between the two is rather weak. Daily ZI is compared against daily aggregate sinuosity for all DJF days in the time series in Fig. 7b. The two variables are correlated at -0.54 at the 99.9% significance level.

b. Annual cycle of sinuosity

The annual cycle of waviness is another aspect of the large-scale behavior of the mid-latitude atmosphere that can be interrogated using sinuosity. An annual cycle of the aggregate sinuosity was constructed by taking each calendar day's average sinuosity over the 66-year time series. The results of this analysis are shown in Fig. 8. Immediately apparent is the fact that the aggregate sinuosity

reaches its maximum in summer and its minimum in winter. In fact, there is a broad peak in waviness that characterizes the warm season (April to October) with peak values of S_5 near 1.9 in early July and a fairly flat period of minimum values (~1.45) occurring in DJF. Also of note is the slight asymmetry in sinuosity on either side of the peak value manifest in a secondary peak in early September. Finally, the annual cycle of 500 hPa zonal index is overlaid with the daily average S_5 in Fig. 8 indicating the nearly perfect inverse relationship between aggregate sinuosity and 500 hPa zonal wind speeds (they are correlated at r = -0.9506).

The annual cycle of sinuosity for the 5 individual isohypses that compose the aggregate are shown, along with the aggregate, in Fig. 9. There is a clear dichotomous structure exhibited amongst these 5 time series. The 576 dm isohypse (red) exhibits the smallest annual cycle in waviness with evidence of two separate peaks, the most prominent one near August 1 and a secondary peak near mid-October. The 564 dm isohypse (orange) is characterized by the sharpest peak (maximizing in early July) but the tails of its annual cycle are not symmetric. The sinuosity is much lower (near 1.3) from January ~15 March whereas it persists well above 1.3 from mid-October to the end of December. A broad warm-season peak also characterizes the 552 dm isohypse (blue) though it reaches its peak value in mid-June. The warm season increase in sinuosity of this streamline also demonstrates a double peak with the secondary maximum centered around August 1.

294 It must be noted that the calculation of daily average sinuosity for
295 individual isohypses includes only those days on which a value exists. This method
296 ensures that whenever the contour does not exist on a given day, its absence does
297 not dilute the average value of sinuosity for the calendar day. This is an important
298 qualification when considering the dramatically different annual cycles exhibited by
299 the 540 (green) and 528 dm (magenta) isohypses (Fig. 9). The areal extent of both
300 of these values of geopotential height shrinks dramatically in the warm season. In
301 fact, for a number of calendar days in late July, more than half of all years had a
302 lower troposphere warm enough to preclude the existence of the 528 dm isohypse.
303 Though this is not the case for the 540 dm isohypse[7], it displays a similar annual
304 cycle of sinuosity. Careful examination of its annual distribution shows that with the
305 approach of summer, the 540 dm isohypse, characterized in winter and spring by a
306 broad polar cap with occasional cutoff "satellites" at low latitude, is transformed
307 into a collection of small, isolated cutoffs. The daily number of distinct 540 dm
308 cutoffs peaks in late May/early June. With continued warming of the hemisphere,
309 the number and areal extent of the 540 dm cutoffs is reduced through July almost to
310 the point of extinction. The reduction in the number and size of 540 dm features,
311 which drastically shrinks the total 540 dm perimeter, greatly reduces the sinuosity
312 of that streamline in July.

313 *c. Relation of the annual cycle in S_5 to morphological features of the NH*
314 *circulation*

[7] July 25 is the calendar day with the highest number (3) of missing 540 dm isohypses. In the entire 66-year time series, there are a total of only 28 such days for 540 dm whereas there are 1934 such days for 528 dm.

315 Cut-off lows (COLs) are closed cyclonic circulations in the upper
316 troposphere that have become detached from, and often subsequently migrate
317 equatorward of, the main westerlies (Gimeno et al. 2007). Conversely, cutoff highs
318 (COHs) are closed anticyclonic circulations that migrate poleward, often as a result
319 of wave breaking, and can promote the development of blocked flows. As described
320 previously, our calculation of sinuosity takes explicit account of the contributions
321 from COLs as well as COHs. Such features invariably increase the sinuosity of a
322 given geopotential height contour to a degree dependent on the areal extent and
323 latitude of the cutoff and so contribute to increases in S_5 as well.

324 The seasonal cycle of aggregate sinuosity is consistent with the higher
325 incidence of mid-tropospheric COLs that characterizes the Northern Hemisphere
326 warm season (Parker et al. 1989, Bell and Bosart 1989, Wernli and Sprenger 2007,
327 Nieto et al. 2008). In fact, Nieto et al. (2008) found that 41% of all COLs identified in
328 the NCEP Reanalysis data from 1948-2006 occurred in JJA while only 17% occurred
329 in DJF. Additionally they found that the frequency of autumn (SON) COLs slightly
330 exceeds that of spring (see their Fig. 14). This is consistent with the secondary peak
331 in S_5 that appears in September/October in the present analysis (see Fig. 6).

332 Parker et al. (1989) also considered the distribution of 500 hPa closed
333 anticyclones in their 36 year climatology. Such features are substantially less
334 frequent than COLs. Though anticyclones needn't be closed to have a substantial
335 impact on sinuosity (e.g. high amplitude, open ridges greatly increase S_5), they found

that these disturbances are most frequent over the subtropics with highest incidence in the warm season.

In order to quantify the contribution of cutoff isohypses to the annual cycle of S_5, COLs and COHs in each of the 5 threshold isohypses were objectively identified over the entire time series. We then recalculated S_5, excluding the influence of the cutoffs. Since COLs are separated from the broader polar cap of heights below a given threshold (Fig. 10a), the areal extent of such features was excluded from the recalculation of equivalent latitude and the contour length around them was excluded from the recalculation of the total contour length[8]. Since a COH is always poleward of the southernmost edge of the distribution of a given isohypse (Fig. 10b), its presence contributes nothing to the area enclosed by that isohypse. Consequently, for COHs no adjustment to equivalent latitude was required - instead, only the length around COHs was excluded in the recalculation of S_5. The annual cycle of the recalculated S_5 is shown along with the actual annual cycle in Fig. 11. The analysis demonstrates that the presence of cutoffs in the warm season produces a substantial increase in sinuosity. In fact, using the wintertime minimum in average S_5 (1.41) as a baseline, cutoffs contribute ~31% to waviness at the peak of the warm season (~July 1).[9] This influence is consistent with the much higher frequency of both species of cutoffs during the warm season. Additionally, routine perusal of 500 hPa maps makes clear that cutoffs nearly always develop within

[8] In addition, any isolated, continuous piece of the area enclosed by a given isohypse that was less than 62% of the total area enclosed by that isohypse on a given day was considered a COL.

[9] This influence was calculated as (S_5 – S_5 w/out cutoffs)/(S_5 – 1.41) which, for peak values near July 1, was 0.15/0.49.

356 flows characterized by elevated values of pre-cutoff waviness. Thus, the evidence
357 presented in Fig. 11 suggests that the development of cutoffs enhances the waviness
358 of the already wavier flow that characterizes the warm season.

359 The coincidence of these various synoptic-climatological features suggests
360 the following explanation for the seasonal cycle in sinuosity. As the minimally wavy
361 wintertime circumpolar vortex shrinks with the coming spring, cutoff lobes of low
362 geopotential height are orphaned at low latitudes where increasingly intense
363 insolation quickly relaxes their associated tropospheric cold anomalies and
364 corresponding negative 500 hPa height anomalies. The warm season maximum in
365 COLs and COHs accounts for a substantial portion of the summertime maximum in
366 S_5. The late summer/early autumn presence of tropical cyclones, and their
367 inevitable recurvature to middle-latitudes, provides a seasonally unique mechanism
368 for the growth of mid-latitude ridges in that season that accounts for the secondary
369 autumnal peak in sinuosity previously noted. Finally, it is hypothesized that the
370 decline of sinuosity in the autumn transition to winter is a function of the absorption
371 of cutoffs that results from the expansion of the circumpolar vortex as the
372 hemisphere cools.

373 **4. Discussion and Conclusions**

374 Despite the fact that a substantial fraction of high-impact, mid-latitude
375 weather events and regimes is associated with large-amplitude planetary waves
376 (Screen and Simmonds 2014), no particular metric for quantifying the waviness of
377 the circulation is widely used. In this paper we have introduced the concept of

sinuosity as a new tool for measuring waviness and applied it to a set of 500 hPa geopotential height contours that contain the maximum wind throughout the year.

A seasonality in the sinuosity of the flow has been demonstrated, with a maximum in summer and minimum in winter. This finding is consistent with the metric of high-amplitude wave patterns introduced by Francis and Vavrus (2015), which exhibits a similar annual cycle to that of S_5. Though conceptual similarities exist between sinuosity and various other metrics of waviness, their respective characterizations of the nature of the mid-latitude flow are not always congruent. For instance, though LWA, like sinuosity, is inversely correlated with zonal wind speed, it exhibits a maximum during winter while effective diffusivity, like sinuosity, is largest during summer.

It has also been demonstrated that a weakening of the mid-tropospheric zonal wind is often associated with an increase in sinuosity. Additionally, a strong negative correlation exists between the observed daily sinuosity and the daily Arctic Oscillation (AO) index in the cold season. Further, the winter (DJF) average sinuosity is shown to be highly correlated with the seasonal average AO and the zonal index (ZI), suggesting that the physical mechanisms that reduce (increase) the poleward height gradient and correspondingly weaken (strengthen) the mid-latitude westerlies, may also foster increased (reduced) waviness.

We have calculated sinuosity based on 500 hPa height contours in this study as a means of characterizing the waviness of the broad, middle tropospheric flow. An extension of the method outlined here, that would more specifically assess the

waviness of the tropopause-level jet stream, would be to calculate the sinuosity of contours of constant potential vorticity (PV) (referred to as *isertels* by Morgan and Nielsen-Gammon 1998). Since the tropopause-level jet is coincident with strong gradients in PV and is found on the low PV edge of such a gradient, calculation of the sinuosity of, for instance, the 2 PVU isertel would render a clear picture of the waviness of the tropopause-level jet stream itself. Complicating matters is the fact that two distinct species of tropopause-level jets, the polar and subtropical jet, are present through much of the year. Isolation of one from the other can be accomplished through consideration of the isertels in separate isentropic layers that contain the separate jets. We plan to pursue this issue in future work.

Recent studies by Francis and Vavrus (2012, 2015), Barnes (2013), and Screen and Simmonds (2013) have examined the question of whether Arctic amplification has caused planetary-scale waves to become wavier and less progressive resulting in more frequent blocking and associated persistent weather regimes. The question remains an open one at present. Continued refinement of the sinuosity metric introduced here promises to enlighten that debate as well as other questions regarding the complexion of the middle-tropospheric flow in a changing climate. To that end, we are currently exploring the nature of the response in sinuosity to a variety of climate change scenarios using output from the CMIP5 suite of models and targeted modeling experiments.

Acknowledgements: This work was supported by the National Science Foundation under a number of grants. J. Martin was supported NSF Grant ATM-1265182. S.

422 Vavrus and F. Wang were supported by NSF Grant ARCSS-1304398 and J. Francis
423 was supported by NSF Grant ARCSS-1304097.

424

REFERENCES

Angell, J. K., 1998: Contraction of the 300 mbar north circumpolar vortex during 1963-1997 and its movement into the Eastern Hemisphere. *J. Geophys. Res.*, **103**, 25887-25893.

Austin, J. F., 1980: The blocking of middle latitude westerly winds by planetary waves. *Quart. J. Roy. Meteor. Soc.*, **106**, 327-350.

Archer, C. L., and K. Caldeira, 2008: Historical trends in the jet streams. *Geophys. Res. Lett.*, **35**, L08803, doi:10.1029/2008GL033614.

Barnes, E. A., E. Dunn-Sigouin, G. Masato, and T. Woollings, 2014: Exploring recent trends in Northern Hemisphere blocking. *Geophys. Res. Lett.*, **41**, doi:10.1002/2013GL058745.

Barnes, E. A., 2013: Revisiting the evidence linking Arctic amplification to extreme weather in midlatitudes. *Geophys. Res. Lett.*, **40**, 1-6, doi:10/1002/GRL.50880.

Bell, G. D., and L. F. Bosart, 1989: A 15-year climatology of Northern Hemisphere 500 mb closed cyclone and anticyclone centers. *Mon. Wea. Rev.*, **117**, 2141-2163.

Bezeau, P., M. Sharp, and G. Gascon, 2014: Variability in summer anticyclonic circulation over the Canadian Arctic Archipelago and west Greenland in the

late 20th/early 21st centuries and its effect on glacier mass balance. *Int. J. of Clim*., doi:10.1002/joc.4000.

Burnett, A. W., 1993: Size variations and long-wave circulation within the January Northern Hemisphere circumpolar vortex: 1946-89. *J. Climate*, **6**, 1914-1920.

Chen, G., J. Lu, A. Burrows, and L. R. Leung, 2015: Local finite-amplitude wave activity as an objective diagnostic of midlatitude extreme weather*, Geophys. Res. Lett.,* **42***,* 10,952–10,960.

Davini, P., C. Cagnazzo, and J. A. Anstey, 2014: A blocking view of the stratosphere-troposphere coupling. *J. Geophys. Res*., **119(19)**, 11100-11115.

Davini, T. D., 2013: Atmospheric blocking and mid-latitude climate variability. Ph. D. dissertation, *Programme in Science and Management of Climate Change*, University of Foscari, Italy.

Davis, R. E., and S. R. Benkovic, 1992: Climatological variations in the Northern Hemisphere circumpolar vortex in January. *Theoretical and Applied Climatology*, **46**, 63-73.

Dole, R. M., and N. D. Gordon, 1983: Persistent anomalies of the extratropical Northern Hemisphere wintertime circulation: Geographical distribution and regional persistence characteristics. *Mon. Wea. Rev*., **111**, 1567-1586.

Egger, J., 1978: Dynamics of blocking highs. *J. Atmos. Sci*., **35**, 1788-1801.

Elliot, R. D., and T. B. Smith, 1949: A study of the effect of large blocking highs on the general circulation in the northern hemisphere westerlies. *J. Meteor*., **6**, 67-85.

Francis, J. A., and S. J. Vavrus, 2012: Evidence linking Arctic amplification to extreme weather in mid-latitudes. *Geophys. Res. Lett*., **39(6)**, L06801, doi:10/1029/2012GL051000.

_____, and _____, 2015: Evidence for a wavier jet stream in response to rapid arctic warming. *Environ. Res. Lett*., **10**, 014005, doi:10.1088/1748-9326/10/1/014005.

Frauenfeld, O. W., and R. E. Davis, 2003: Northern Hemisphere circumpolar vortex trends and climate change implications. *J. Geophys. Res*., **108**, 4423-doi:10.1029/2002/JD002958.

Gimeno, L., R. M. Triego, P. Ribera, and J. A. Garcia, 2007: Editorial: Special issue on cut-off low systems (COL). *Meteorol. Atmos. Phys*., **96**, 1-2, doi:10.1007/s00703-006-0216-5.

Haynes, P., and E. Shuckburgh, 2000a: Effective diffusivity as a diagnostic of atmospheric transport: 1. Stratosphere. *J. Geophys. Res*., **105**, 22777-22794.

_____, and _____, 2000b: Effective diffusivity as a diagnostic of atmospheric transport: 2. Troposphere and lower stratosphere. *J. Geophys. Res*., **105**, 22795-22810.

Huang, C. S. Y., and N. Nakamura, 2016: Local finite-amplitude wave activity as a diagnostic of anomalous weather events. *J. Atmos. Sci*., **73**, 211-229.

485 Kalnay, E. et al., 1996: The NCEP/NCAR 40-year reanalysis project. *Bull. Amer.*
486 *Meteor. Soc.*, **77**, 437-471.

487 Lejenäs, H., and H. Øakland, 1983: Characteristics of northern hemisphere blocking
488 as determined from long time series of observational data. *Tellus*, **35A**, 350-
489 362.

490 Leopold. L. B., M. G. Wolman, and J. Miller, 1964: *Fluvial processes in geomorphology*.
491 W. H. Freeman & Co., San Francisco, 522 p.

492 Lupo, A. R., and P. J. Smith, 1995: Climatological features of blocking anticyclones in
493 the Northern Hemisphere. *Tellus*, **47A**, 439-456.

494 Markham, C. G., 1985: A quick and direct method for estimating mean monthly
495 global temperatures from 500 mb data. *Professional Geographer*, **37**, 72-74.

496 Martin, J. E., 2015: Contraction of the Northern Hemisphere, lower tropospheric,
497 wintertime cold pool over the last 66 years. *J. Climate*, **28**, 3764-3778.

498 Masato, G., B. J. Hoskins, and T. J. Woollings, 2013: Winter and summer Northern
499 Hemisphere blocking in CMIP5 models. *J. Climate*, **26**, 7044-7059.

500 Morgan, M. C., and J. W. Nielsen-Gammon, 1998: Using tropopause maps to diagnose
501 midlatitude weather systems. *Mon. Wea. Rev*., **126**, 2555-2579.

502 Nakamura, N., 1996: Two-dimensional mixing, edge formation, and permeability
503 diagnosed in an area coordinate. *J. Atmos. Sci*., **53**, 1524-1537.

_____, and D. Zhu, 2010: Finite-amplitude wave activity and diffusive flux of potential vorticity in eddy-mean flow interaction. *J. Atmos. Sci*., **67**, 2701-2716.

_____, and A. Solomon, 2010: Finite-amplitude wave activity and mean flow adjustments in the atmospheric general circulation. Part I: Quasigeostrophic theory and analysis. *J. Atmos. Sci*., **67**, 3967-3983.

_____, and _____, 2011: Finite-amplitude wave activity and mean flow adjustments in the atmospheric general circulation. Part II: Analysis in the isentropic coordinate. *J. Atmos. Sci*., **68**, 2783-2799.

Namias, J., 1950: The index cycle and its role in the general circulation. *J. Meteor*., **7**, 130-139.

_____, 1947a: Physical nature of some fluctuations in the speed of the zonal circulation. *J. Meteor*., **4**, 125-133.

_____, 1947b: Characteristics of the general circulation over the northern hemisphere during the abnormal winter of 1946-47. *Mon. Wea. Rev*., **75**, 145-152.

Nieto, R., M. Sprenger, H. Wernli, R. M. Triego, and L. Gimeno, 2008: Identification and climatology of cut-off lows near the tropopause. *Trends and Directions in Climate Research:* Ann. N. Y. Acad. Sci. 1146: 256-290, doi:101196/annals.1446.016.

524 Parker, S. S., J. T. Hawes, S. J. Colucci, and B. P. Hayden, 1989: Climatology of 500 mb
525 cyclones and anticyclones, 1950-85. *Mon. Wea. Rev*., **117**, 558-570.

526 Pelly, J., and B. J. Hoskins, 2003: A new perspective on blocking. *J. Atmos. Sci*., **60**,
527 743-755.

528 Rex, D. F., 1950a: Blocking action in the middle troposphere and its effect upon
529 regional climate. Part I: An aerological study of blocking action. *Tellus*, **2**, 196-
530 211.

531 _____, 1950b: Blocking action in the middle troposphere and its effect upon
532 regional climate. Part II: The climatology of blocking action. *Tellus*, **2**, 275-
533 301.

534 Rohli, R. V., K. M. Wrona, and M. J. McHugh, 2005: January northern hemisphere
535 circumpolar vortex variability and its relationship with hemispheric
536 temperature and regional teleconnections. *Int. J. Climatol*., **25**, 1421-1436.

537 Rossby, C.-G., and collaborators, 1939: Relations between variations in the intensity
538 of the zonal circulation of the atmosphere and the displacements of the semi-
539 permanent centers of action. *J. Marine Res*., **2**, 38-54.

540 Schwierz, C., M. Croci-Maspoli, and H. C. Davies, 2004: Perspicacious indicators of
541 atmospheric blocking. *Geophys. Res. Lett*., **31**, L06125,
542 doi:10.1029/2003GL019341.

543 Screen, J. A., and I. Simmonds, 2013: Exploring links between Arctic amplification
544 and mid-latitude weather. *Geophys. Res. Lett.*, **40**, 1-6,
545 doi:10.1002/GRL.50174.

546 _____, and _____, 2014: Amplified mid-latitude planetary waves favour particular
547 regional weather extremes. *Nat. Clim. Change*, **4**, 704-709.

548 Shabbar, A., J. Huang, and K. Higuchi, 2001: The relationship between the wintertime
549 North Atlantic Oscillation and blocking episodes in the North Atlantic. *Int. J.*
550 *Climatol.*, **21**, 355-369.

551 Wernli, H., and M. Sprenger, 2007: Identification and ERA-15 climatology of
552 potential vorticity streamers and cutoffs near the extratropical tropopause*. J.*
553 *Atmos. Sci.*, **64**, 1569-1586.

554 Wexler, H., 1948: A note on the record low temperature in the Yukon Territory
555 January-February 1947. *Bull. Amer. Meteor. Soc.*, **29**, 547-550.

556 White, W. B., and N. E. Clark, 1975: On the development of blocking ridge activity
557 over the central North Pacific. *J. Atmos. Sci.*, **32**, 489-502.

558 Willett, H. C., 1948: Pattersn of world weather changes. *Trans. Amer. Geophys. Union*,
559 **29**, 803-809.

560 Winters, K. B., and E. A. D'Asaro, 1996: Diascular flux and the rate of fluid mixing. *J.*
561 *Fluid. Mech.*, **317**, 179-193.

562 Woollings, T., J. G. Pinto, and J. A. Santos, 2011: Dynamical evolution of north Atlantic
563 ridges and poleward jet stream displacements. *J. Atmos. Sci*., **68**, 954-963.

564 Wrona, K. M., and R. V. Rohli, 2007: Seasonality of the northern hemisphere
565 circumpolar vortex. *Int. J. Climatol*., **27**, 697-713.

566

Appendix

Circularity ratio (R_C) is defined as $R_C = \frac{A}{EQA}$, where A is the area enclosed by a given isohypse, and EQA is the area of the circle with the same perimeter as the isohypse.

Sinuosity (S) is defined as $S = \frac{L}{EQL}$, where L is the length of the given isohypse, and EQL is the circumference of the circle that encloses the same area as the isohypse.

Expressions for both of the known quantities (A and L, which are calculated from data) in terms of other relevant variables can be formulated. For instance,

$$L = 2\pi R_e \cos\phi_p$$

where ϕ_p is the latitude at which the circumference of a circle around the pole equals the length of the given isohypse. Thus, the variable EQA is given by

$$EQA = 2\pi R_e^{\,2}[1 - \sin\phi_p]$$

and the actual area enclosed by the isohypse is given by

$$A = 2\pi R_e^{\,2}[1 - \sin\phi_e],$$

where ϕ_e is the equivalent latitude derived from the initial calculation of the area enclosed by the isohypse.

Consequently, circularity ratio can be rewritten as

585 $$C = \frac{A}{EQA} = \frac{2\pi R_e{}^2[1-\sin\phi_e]}{2\pi R_e{}^2[1-\sin\phi_p]} = \frac{[1-\sin\phi_e]}{[1-\sin\phi_p]}. \quad \text{(A1)}$$

586

587 Sinuosity can also be rewritten in terms of these two different latitudes as

588 $$S = \frac{L}{EQL} = \frac{2\pi R_e \cos\phi_p}{2\pi R_e \cos\phi_e} = \frac{\cos\phi_p}{\cos\phi_e} \quad \text{(A2)}$$

589 since $EQL = 2\pi R_e \cos\phi_e$ by definition. Thus, the relationship between R_C and S is

590

591 $$S^2 R_c = \frac{1+\sin\phi_p}{1+\sin\phi_e}. \quad \text{(A3)}$$

592 Portraying sinuosity as a function of latitude requires translation of the
593 metric from height coordinates to latitude coordinates. This translation is
594 accomplished in three steps. First, one first calculates daily average SIN for a series
595 of individual geopotential height (Z) contours from 4600m to 6000m at 10m
596 intervals establishing SIN as a function of Z for each day of the 66 year NCEP
597 Reanalysis time series. Next, the daily average geopotential height at each latitude
598 (from 20°N to 90°N) for each day is calculated. Then the daily SIN for a given Z can
599 be assigned to a particular latitude. Finally the 66-year average SIN (at each
600 latitude) is calculated. The results of such a translation are shown in Fig. A1.

601

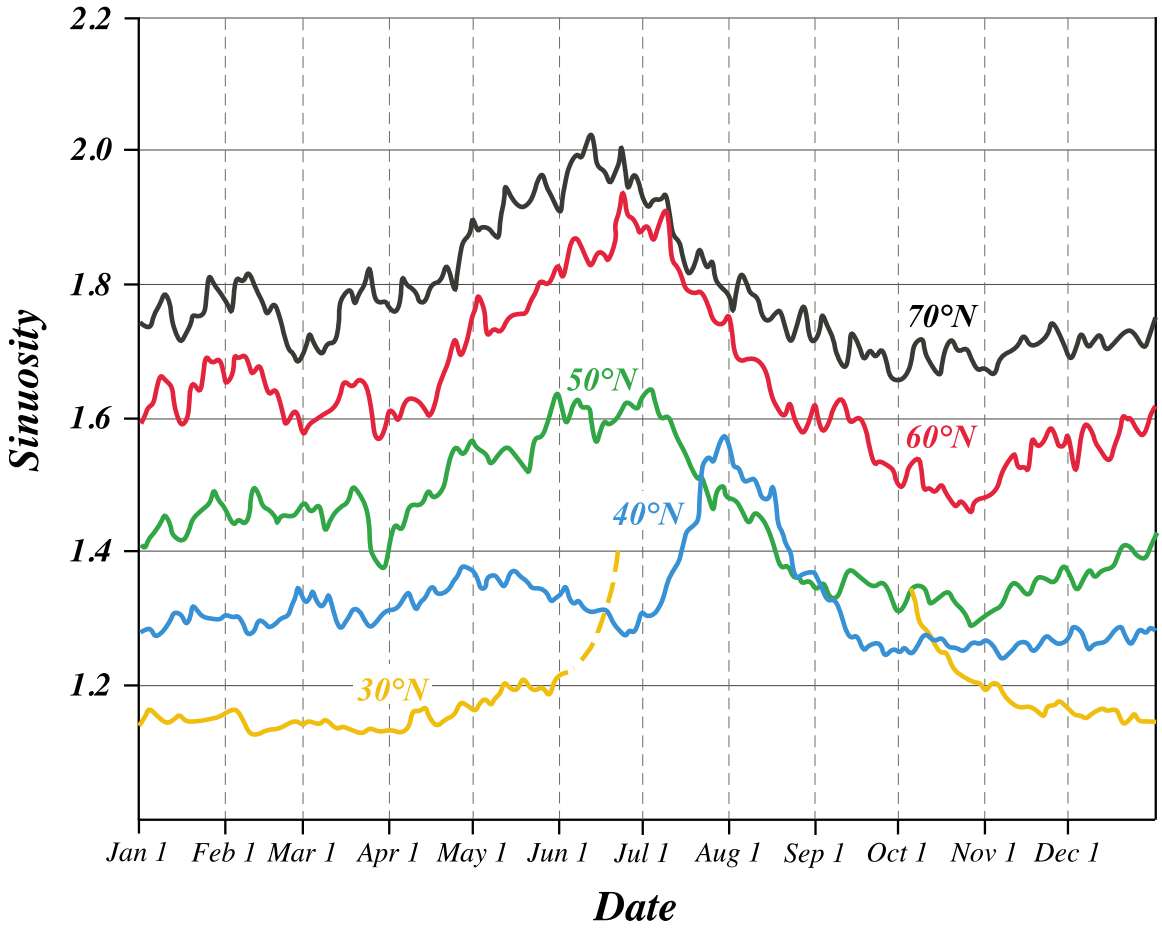

Fig. A1 Annual cycle of 500 hPa sinuosity as a function of latitude. The various latitude bands are labeled with 30°N not calculated through most of June-September as the daily averaged geopotential height at that latitude in those months is often over 6000m.

602

603

604

605

606

606

607 FIGURE CAPTIONS

608 Fig. 1 Schematic illustrating the concept of sinuosity. $\boldsymbol{S_{AB}}$ is the ratio of the length of
609 the blue contour to the length of the red line segment AB.

610 Fig. 2 Blue line is the daily average 552 dm geopotential height contour at 500 hPa
611 on 18 January 2014. The area enclosed by that line is equal to the area enclosed by
612 the red circle (the equivalent latitude). $\boldsymbol{S_{552}}$ is equal to the ratio of the length of the
613 blue line to the length of the red line (1.2719).

614 Fig. 3 Schematic illustration of the negligible effect that poleward migration of
615 isohypses has on sinuosity of a given contour. Original contour (in red) is zonal at
616 35N with a square wave of latitudinal depth 10. Displace contour (in blue) is zonal
617 at 40N with square wave whose aspect ratio (longitudinal extent/latitudinal extent)
618 is identical to original wave. The displaced contour has sinuosity 1.0024 times that
619 of original contour.

620 Fig. 4 Time series of DJF season averaged, aggregate sinuosity from 1948-49 to
621 2013-14.

622 Fig. 5 (a) Time series of correlation coefficient, r, between the daily AO index and
623 the daily value of 500 hPa sinuosity (S_5) from 1950-51 to 2013-14. Green (blue)
624 dots represent seasons with r < -0.4 (-0.6). (b) Scatterplot of daily SIN_5 and daily AO
625 index for every DJF day from 1950-51 to 2013-14. Red line is the regression line
626 and the two variables are correlated at -0.431.

627 Fig. 6 Time series of DJF seasonal averaged AO index (red) compared to DJF
628 seasonal averaged sinuosity (S_5) (blue). The two time series are correlated with r =
629 -0.520, significant above the 99% level.

630 Fig. 7 (a) Time series of correlation coefficient, r, between daily zonal index (ZI) and the
631 daily value of 500 hPa aggregate sinuosity (S5) from 1948-49 to 2013-14. Green (blue)
632 dots represent seasons with r < -0.4 (-0.6). (b) Scatterplot of daily SIN_5 and daily ZI for
633 every DJF day in the 66-year NCEP Reanalysis time series. Red line is the regression
634 line and the two variables are correlated at -0.542.

635 Fig. 8 Daily average aggregate sinuosity (solid black line) derived from 66-year
636 NCEP Reanalysis time series. Gray shaded region represents +/- 1σ around the
637 daily mean. Daily average 500 hPa zonal index (ZI in m s^{-1}, blue solid line) derived
638 from the same data set.

639 Fig. 9 Solid black line is the daily average aggregate sinuosity derived from 66-year
640 NCEP Reanalysis time series. Daily average sinuosity of individual geopotential
641 height contours in the set of 5 used in the aggregate calculation are indicated by the
642 labeled colored lines.

643 Fig. 10 Schematic of an isohypse characterized by (a) a cutoff low (COL) and (b) a cutoff
644 high (COH). The total area enclosed by the given isohypse in both panels is shaded blue.
645 For the COL in (a), that area is the sum of A and B while the total contour length is the
646 sum of the perimeters of A and B. Recalculation of S5 in this case requires subtraction of
647 area B from the total area and subtraction of perimeter B from the total contour length.

For the COH in (b), the total area is smaller. Recalculation of S5 in this case requires only that the perimeter of C be subtracted from the total contour length.

Fig. 11 Solid black line is the daily average aggregate sinuosity derived from 66-year NCEP Reanalysis time series. Gray line represents the daily average sinuosity calculated upon excluding the contribution of cutoff lows and highs in the threshold isohypses. See text for explanation.

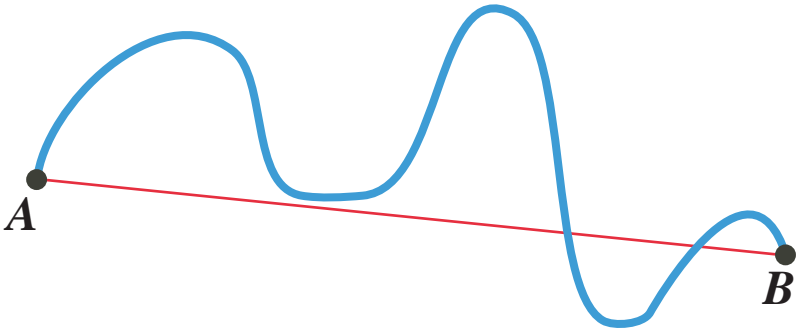

$$S_{AB} = \frac{\text{(Length of CONTOUR)}}{\text{(Length of SEGMENT)}}$$

Fig. 1 Schematic illustrating the concept of sinuosity. S_{AB} is the ratio of the length of the blue contour to the length of the red line segment AB.

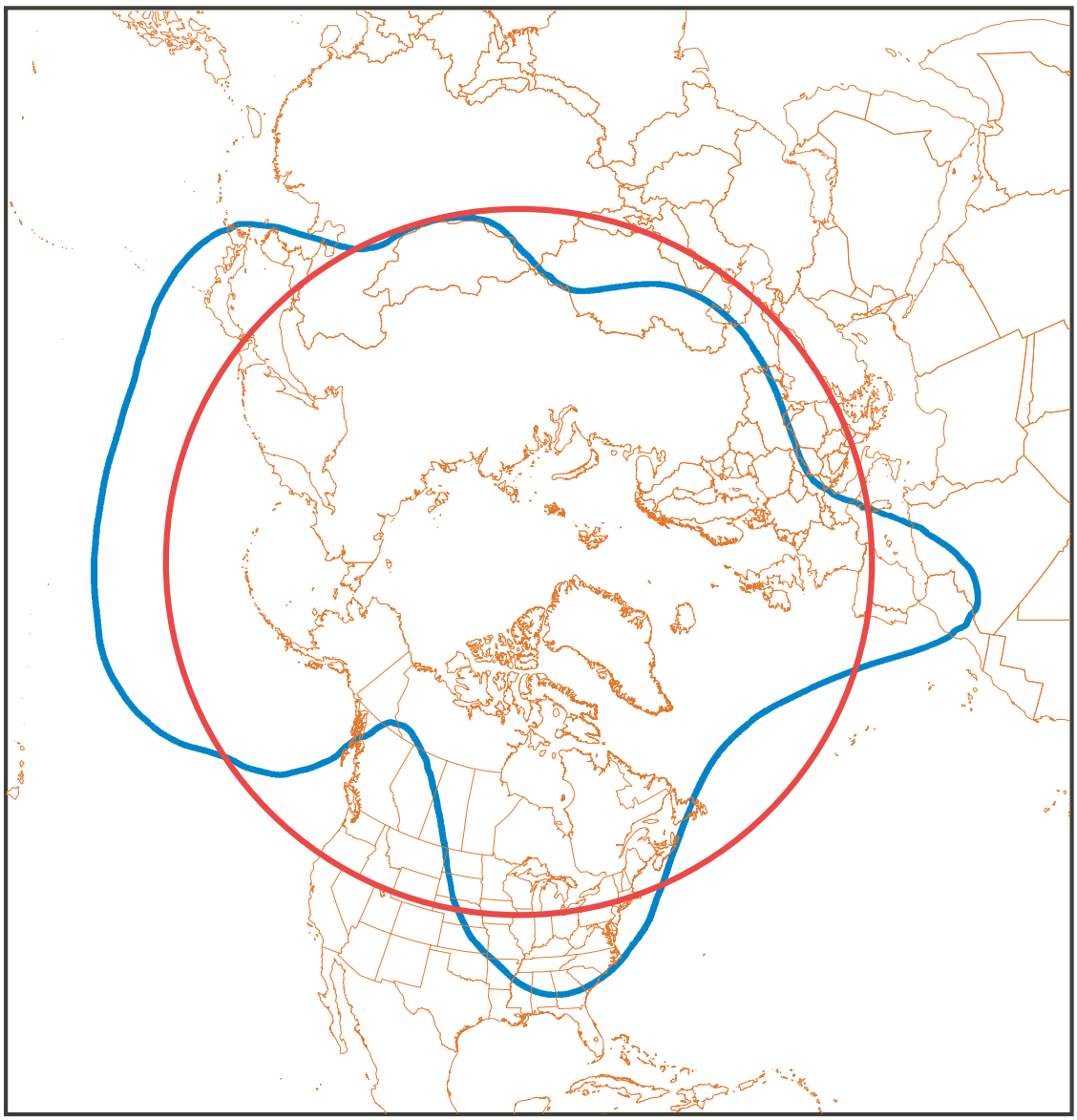

Fig. 2 Blue line is the daily average 552 dm geopotential height contour at 500 hPa on 18 January 2014. The area enclosed by that line is equal to the area enclosed by the red circle (the equivalent latitude). S_{552} is equal to the ratio of the length of the blue line to the length of the red line (1.2719).

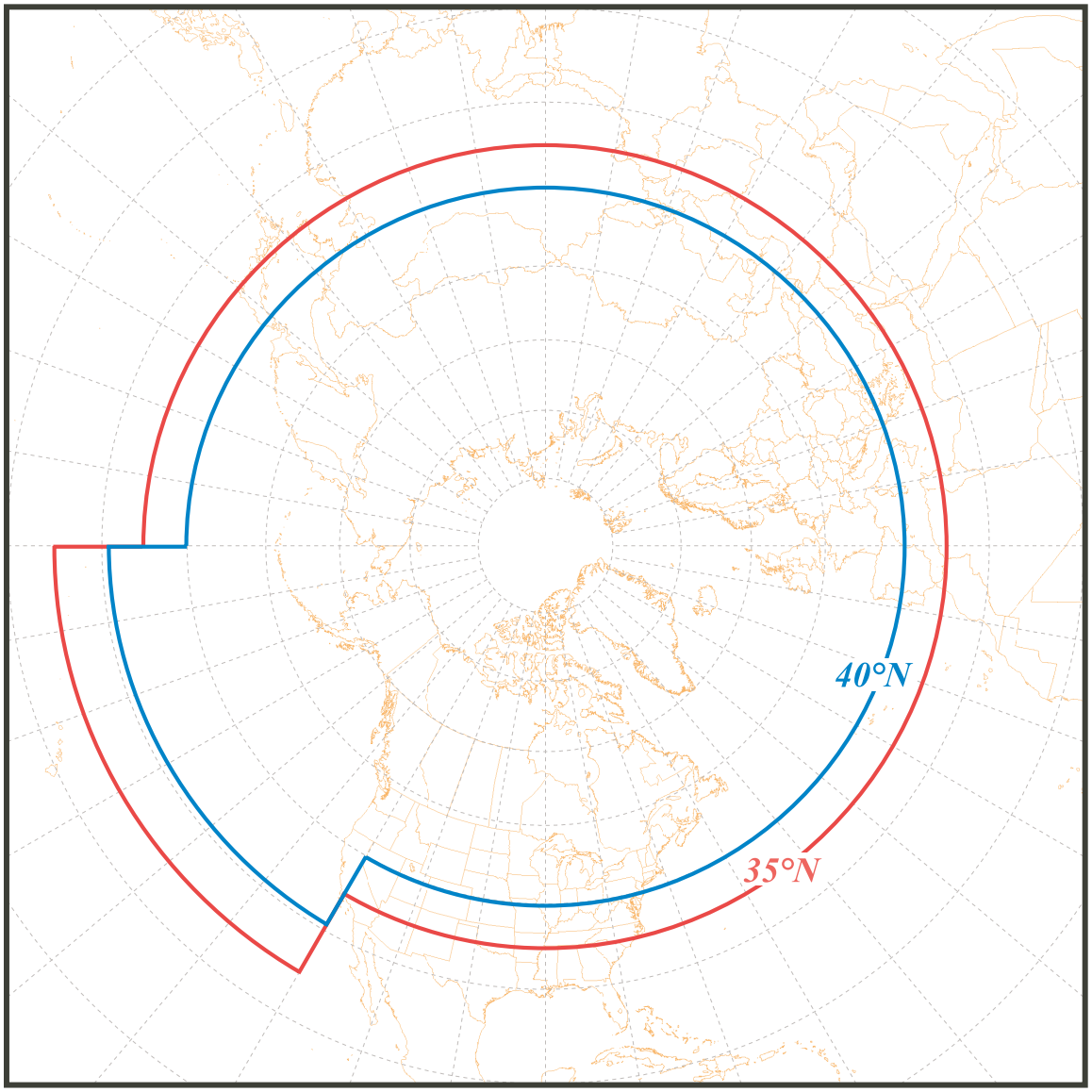

Fig. 3 Schematic illustration of the negligible effect that poleward migration of isohypses has on sinuosity of a given contour. Original contour (in red) is zonal at 35°N with a square wave of latitudinal depth 10°. Displaced contour (in blue) is zonal at 40°N with square wave whose aspect ratio (longitudinal extent/latitudinal extent) is identical to original wave. The displaced contour has sinuosity 1.0024 times that of original contour.

657

658

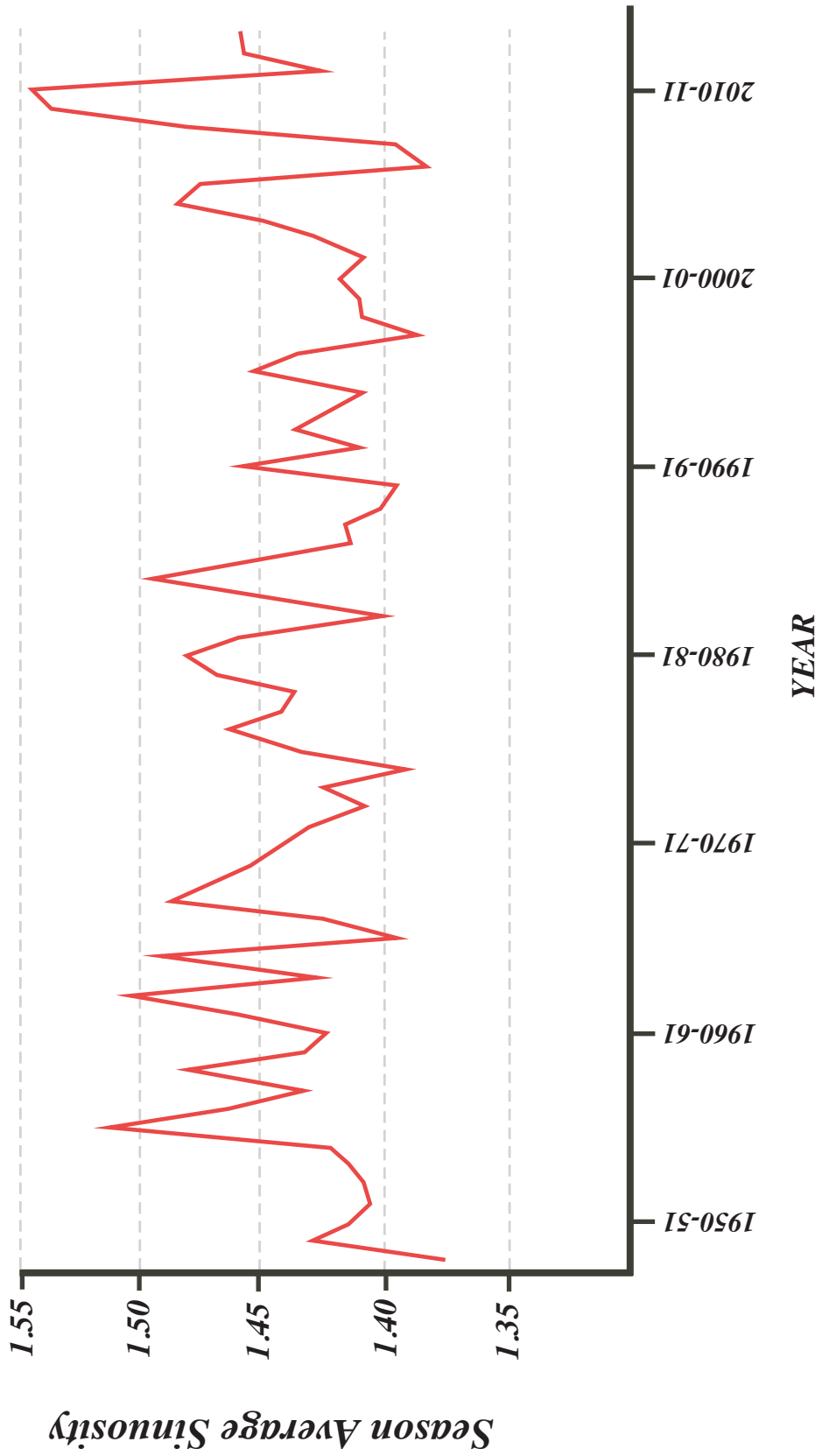

Fig. 4 Time series of DJF season averaged, aggregate sinuosity from 1948-49 to 2013-14.

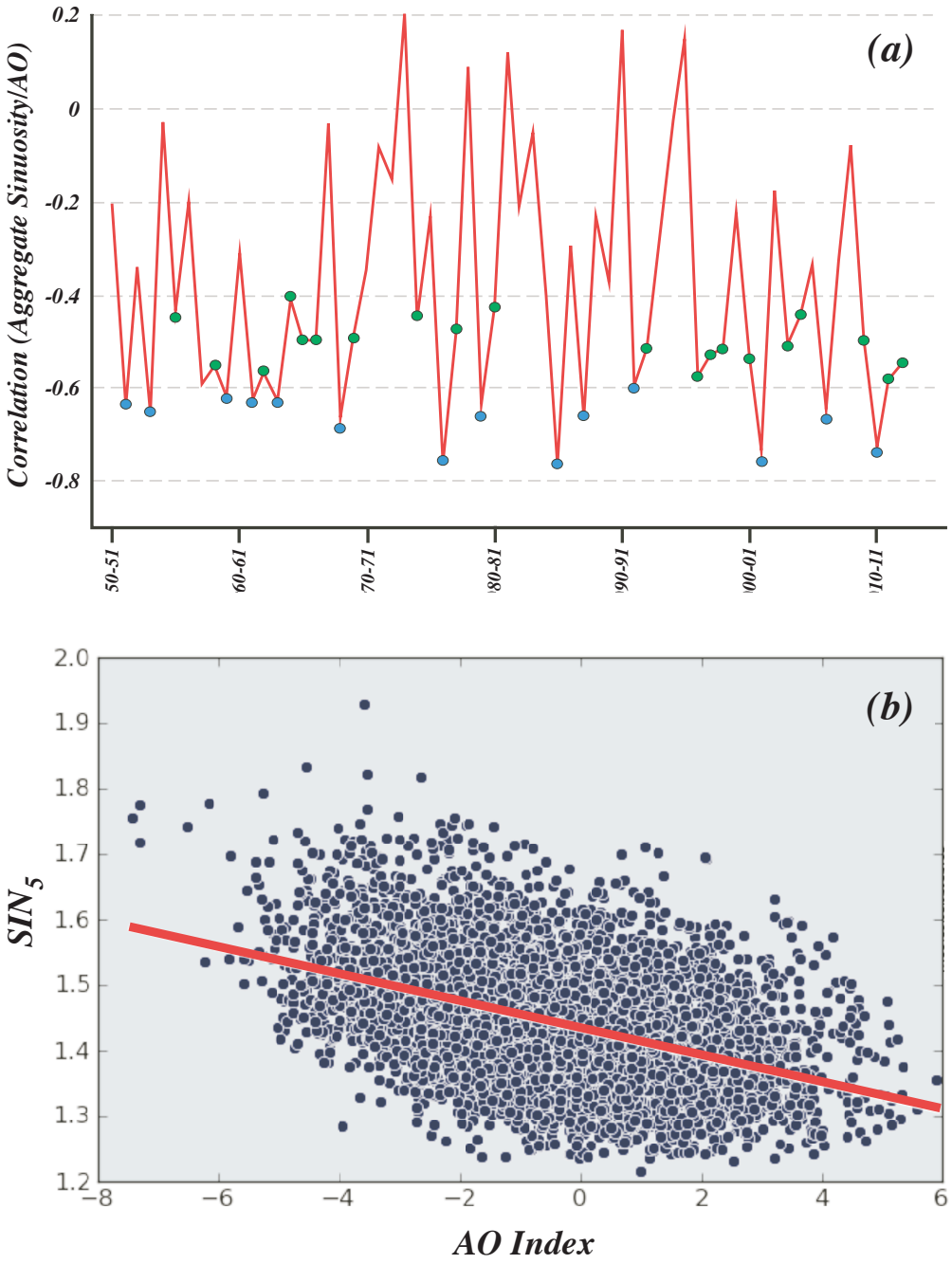

Fig. 5 (a) Time series of correlation coefficient, r, between the daily AO index and the daily value of 500 hPa sinuosity from 1950-51 to 2013-14. Green (blue) dots represent seasons with r < -0.4 (-0.6). (b) Scatterplot of daily SIN5 and daily AO index for every DJF day from 1950-51 to 2013-14. Red line is the regression line and the two variables are correlated at -0.431.

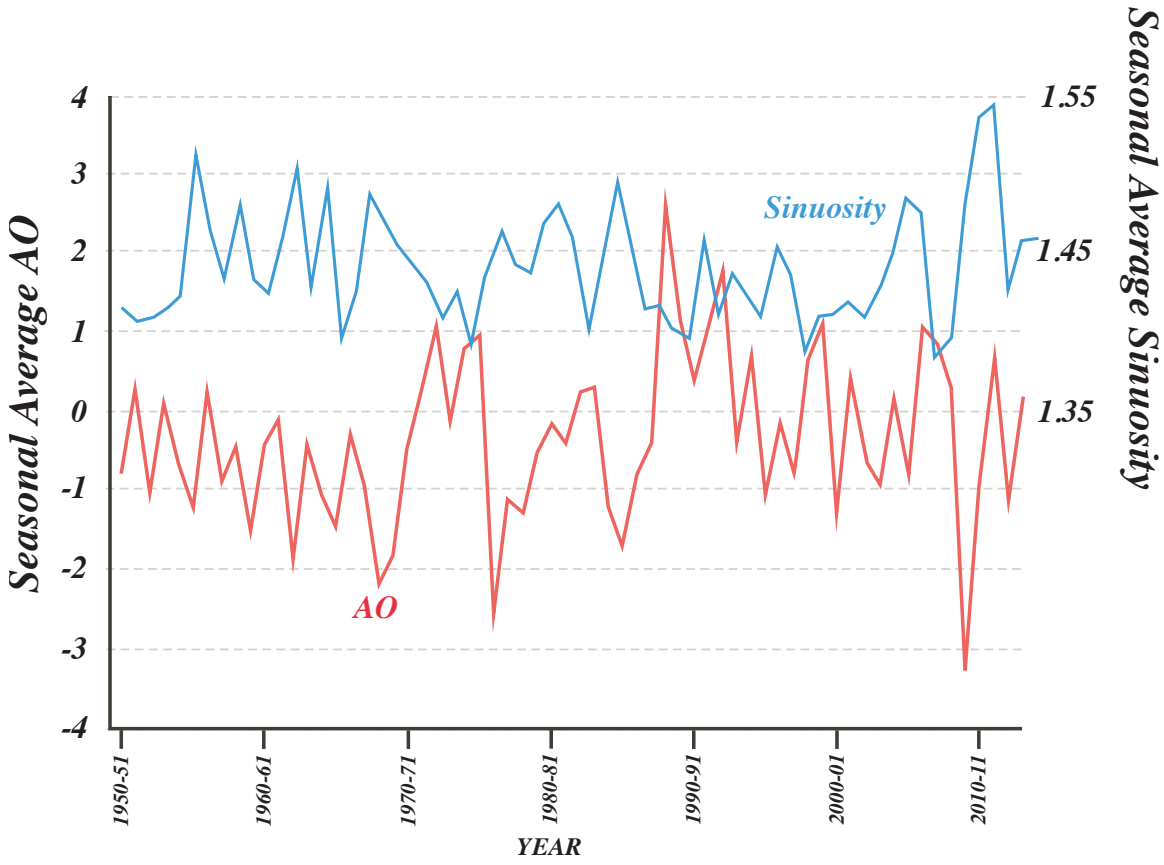

Fig. 6 Time series of DJF seasonal averaged AO index (red) compared to the DJF seasonal averaged sinuosity (blue). The two time series are correlated with r = -0.520, significant above the 99% level.

661

662

662

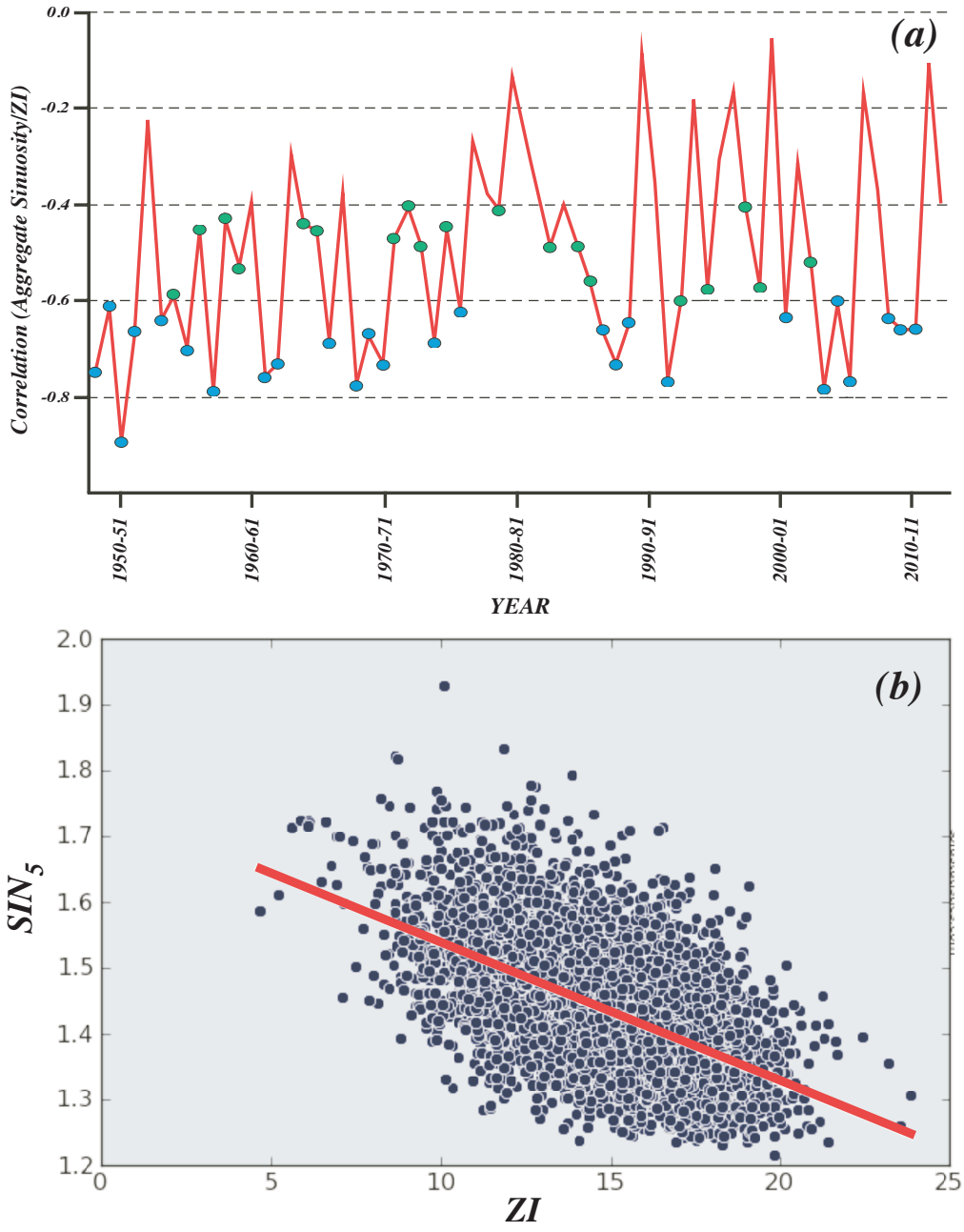

Fig. 7 (a) Time series of correlation coefficient,r, between daily zonal index (ZI) and the daily value of 500 hPa aggregate sinuosity (S5) from 1948-49 to 2013-14. Green (blue) dots represent seasons with r < -0.4 (-0.6). (b) Scatterplot of daily SIN5 and daily ZI for every DJF day in the 66-year NCEP Reanalysis time series. Red line is the regression line and the two variables are correlated at -0.542.

663

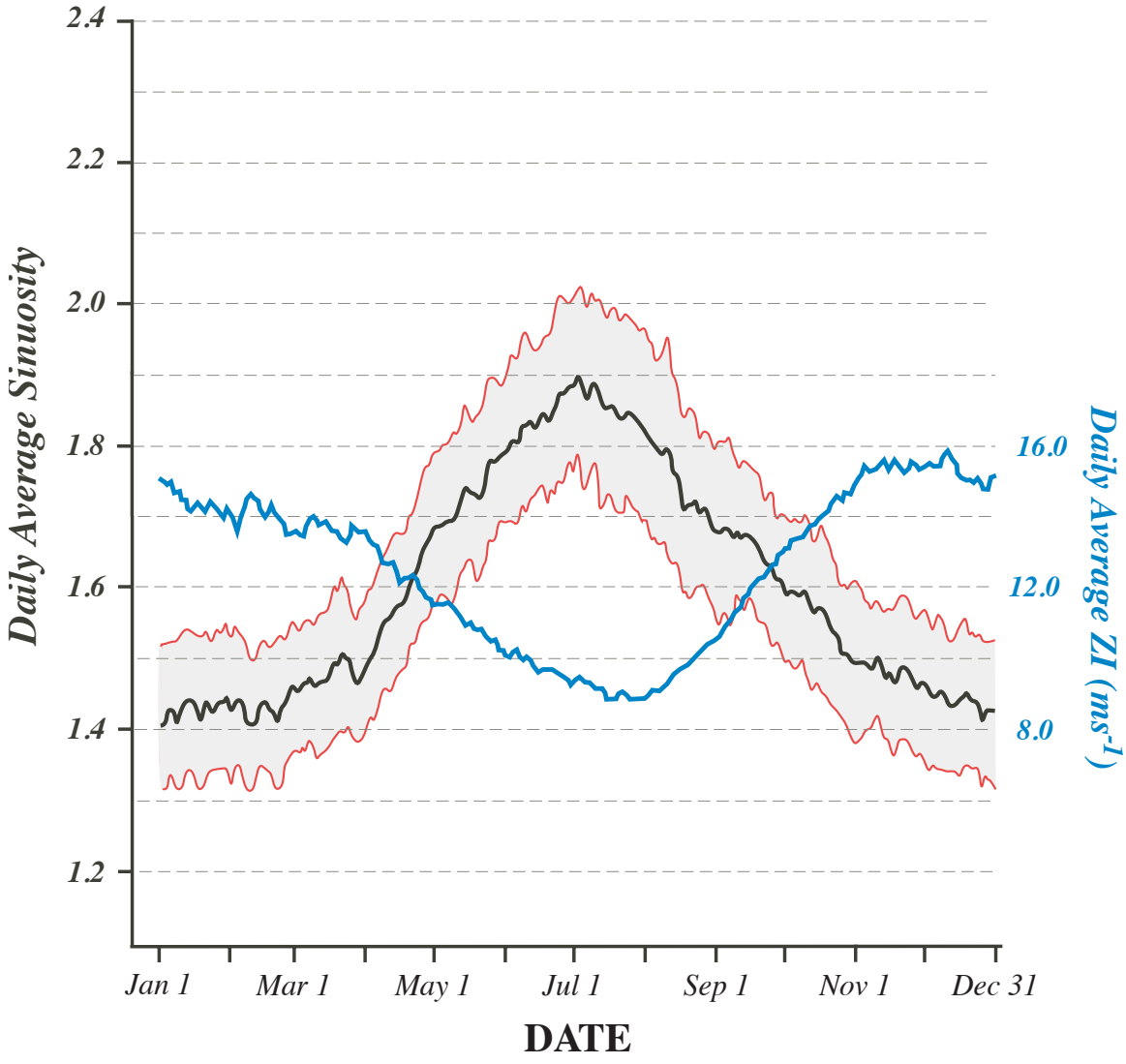

Fig. 8 Daily average aggregate sinuosity (solid black line) derived from 66-year NCEP Reanalysis time series. Gray shaded region represents +/- 1σ around the daily mean. Daily average 500 hPa zonal index (ZI in ms^{-1}, blue solid line) derived from the same data set.

664

665

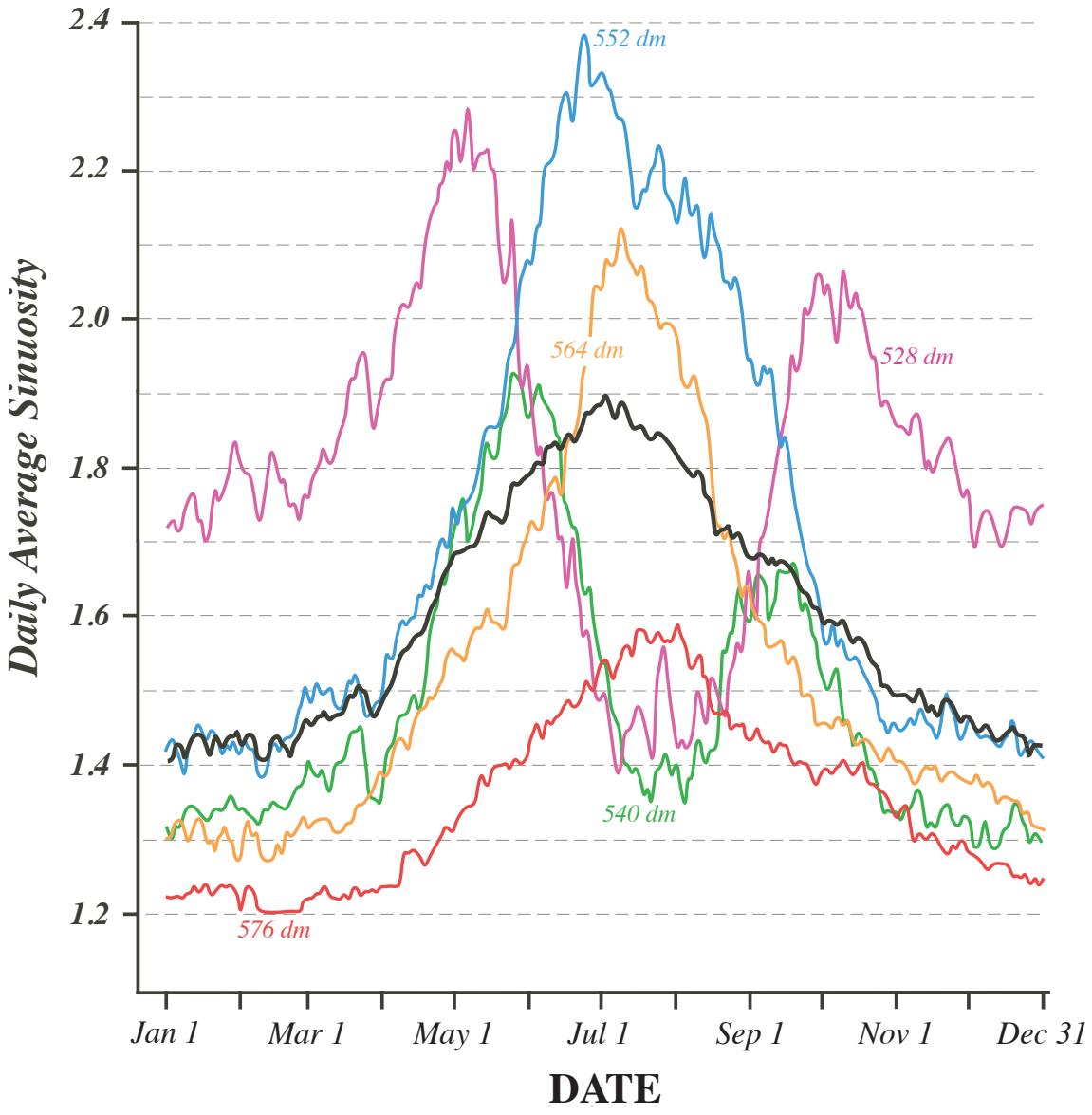

Fig. 9 Solid black line is the daily average aggregate sinuosity derived from 66-year NCEP Reanalysis time series. Daily average sinuosity of individual geopotential height contours in the set of 5 used in the aggregate calculation are indicated by the labeled colored lines.

665

666

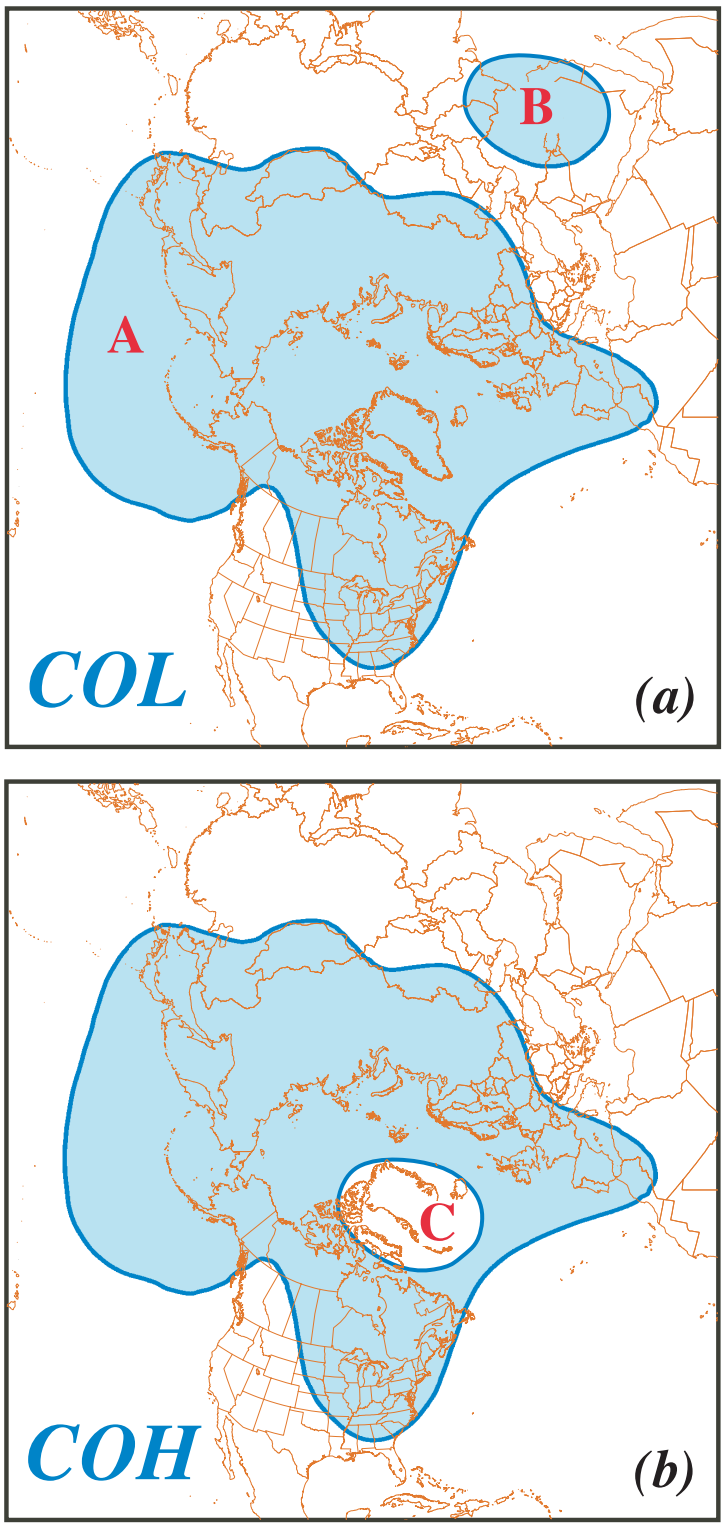

Fig. 10 Schematic of an isohypse characterized by (a) a cutoff low (COL) and (b) a cutoff high (COH). The total area enclosed by the given isohypse in both panels is shaded blue. For the COL in (a), that area is the sum of A and B while the total contour length is the sum of the perimeters of A and B. Recalculation of S_5 in this case requires subtraction of area B from the total area and subtraction of perimeter B from the total contour length. For the COH in (b), the total area is smaller. Recalculation of S_5 in this case requires only that the perimeter of C be subtracted from the total contour length.

666

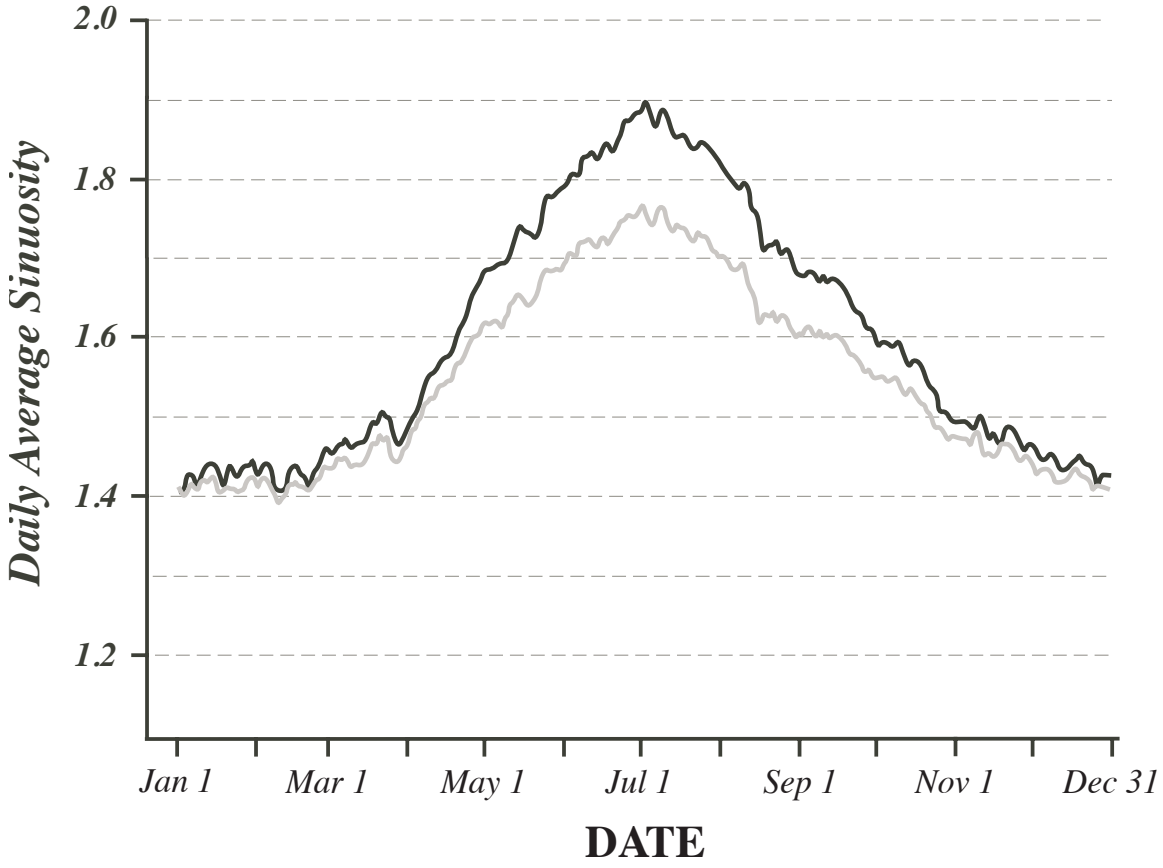

Fig. 11 Solid black line is the daily average aggregate sinuosity derived from 66-year NCEP Reanalysis time series. Gray line represents the daily average sinuosity calculated upon excluding the contribution of cutoff lows and highs in the threshold isohypses. See text for explanation.

667

668

669